JACS
JOURNAL OF THE AMERICAN CHEMICAL SOCIETY
pubs.acs.org/JACS
Article

Sulfate Promotes Amine Salt Ozonation in Atmospheric Aerosols

Weina Zhang, Dayuan Zheng, Jiale Lao, Ruijing Li, Baihang Chen, Jiangyao Chen, Jie Zhong, Yuemeng Ji, Guiying Li, Joseph S. Francisco, and Taicheng An*

Cite This: J. Am. Chem. Soc. 2025, 147, 34327−34338
Read Online
ACCESS | Metrics & More | Article Recommendations | Supporting Information

ABSTRACT: Low molecular weight amines promote sulfate (SO_4^{2-} and HSO_4^-) formation through acid−base reactions, contributing to fine particulate matter (PM). Heterogeneous ozonation converts nontoxic amine salts into highly toxic products, yet the ozonation activation mechanism is unclear. This work reveals a sulfate-dominant ozonation mechanism of amine salts in fine PM by combining advanced mass spectrometry and ab initio calculation methods. With the synergy of •OH-initiated oxidation, SO_4^{2-} activates amine ions through deprotonation, producing imine molecules as ozonation intermediates. Subsequently, HSO_4^- accelerates the formation of the intermediate aminomethanol and ozonation products. Moreover, this novel ozonation mechanism of amine salt is verified to be efficient for sulfate fine PM and is not feasible for chloride or nitrate fine PM. In this study, the key role of sulfate in the ozonation of inert organic compounds is highlighted, which needs to be considered in fine PM chemistry.

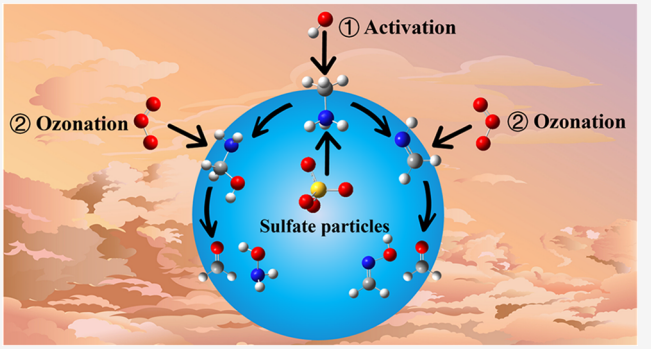

1. INTRODUCTION

Fine particulate matter (PM) is an important component of atmospheric particles[1] and has severe adverse effects on human health.[2,3] New particle formation (NPF) serves as a significant source of atmospheric ultrafine/fine PM.[4,5] Recent studies have indicated that the sulfuric acid−amine−water ternary nucleation mechanism can explain NPF events in typical urban atmospheres,[6−8] as well as in the Antarctic atmosphere.[9] These field measurement studies directly state that amines play key roles in fine PM formation on global scale. During NPF, parent amines are easily converted into amine salts by acid−base neutralization with acidic seeds[10] or displacement with particulate ammonium salts,[11] which subsequently enter the particle phase.

Composite atmospheric pollution events dominated by PM and ozone (O_3) frequently occur worldwide.[12,13] High levels of O_3 and free radicals lead to heterogeneous oxidation of fine PM. Particulate amine salts are initially nontoxic,[14] but the ozonation products of organic amines,[15] including aldehydes, nitrates, amides, and hydroxylamines, are becoming highly toxic.[11,16,17] A large number of field observation studies[18−21] have detected these species in fine PM, which is likely due to the ozonation of particulate-phase organic amines. Indeed, monitoring of aliphatic amines in PM showed that there was a significant negative correlation between amine and ozone, indicating that the ozonation process weakened the abundance of amines.[22] In addition, experimental studies have shown that the hydroxylamine generated from the ozonation of dimethylamine salt can react with dimethylamine to form carcinogenic nitrosodimethylamine, contributing about 10% of the nitrosodi-methylamine production in fine PM during summer.[23] Additionally, research has indicated that, the primary amine ozonation in fine PM in the atmosphere can produce nitroalkanes and amide products.[24] Therefore, elucidating the ozonation mechanism of particulate amine salts is highly important for accurately assessing the environmental health risks of ultrafine/fine PM during composite atmospheric pollution events.

However, large gaps remain in understanding the amine salt ozonation mechanism in fine PM. Unlike the reactivity of molecular parent amines to ozone,[25,26] amine salts are chemically inert to ozone.[27,28] Thus, intermediates with ozonation reactivity are first formed to initiate amine salt ozonation in fine PM. Considering the ozonation reactivity of amine molecules, in one experimental study on trimethylamine salt ozonation, it was suggested that amine salt ions spontaneously revert to parent amine molecules before undergoing ozonation.[11] Unfortunately, this study lacks direct evidence confirming that the proposed reversion readily occurs under ambient conditions (temperature = 298 K). Previous studies have shown that the pK_a of amine salt ions is around 10.7, which means that amine ions are difficult to give protons.[29,30]

Received: March 12, 2025
Revised: July 17, 2025
Accepted: July 25, 2025
Published: September 10, 2025

https://doi.org/10.1021/jacs.5c04343
J. Am. Chem. Soc. 2025, 147, 34327−34338

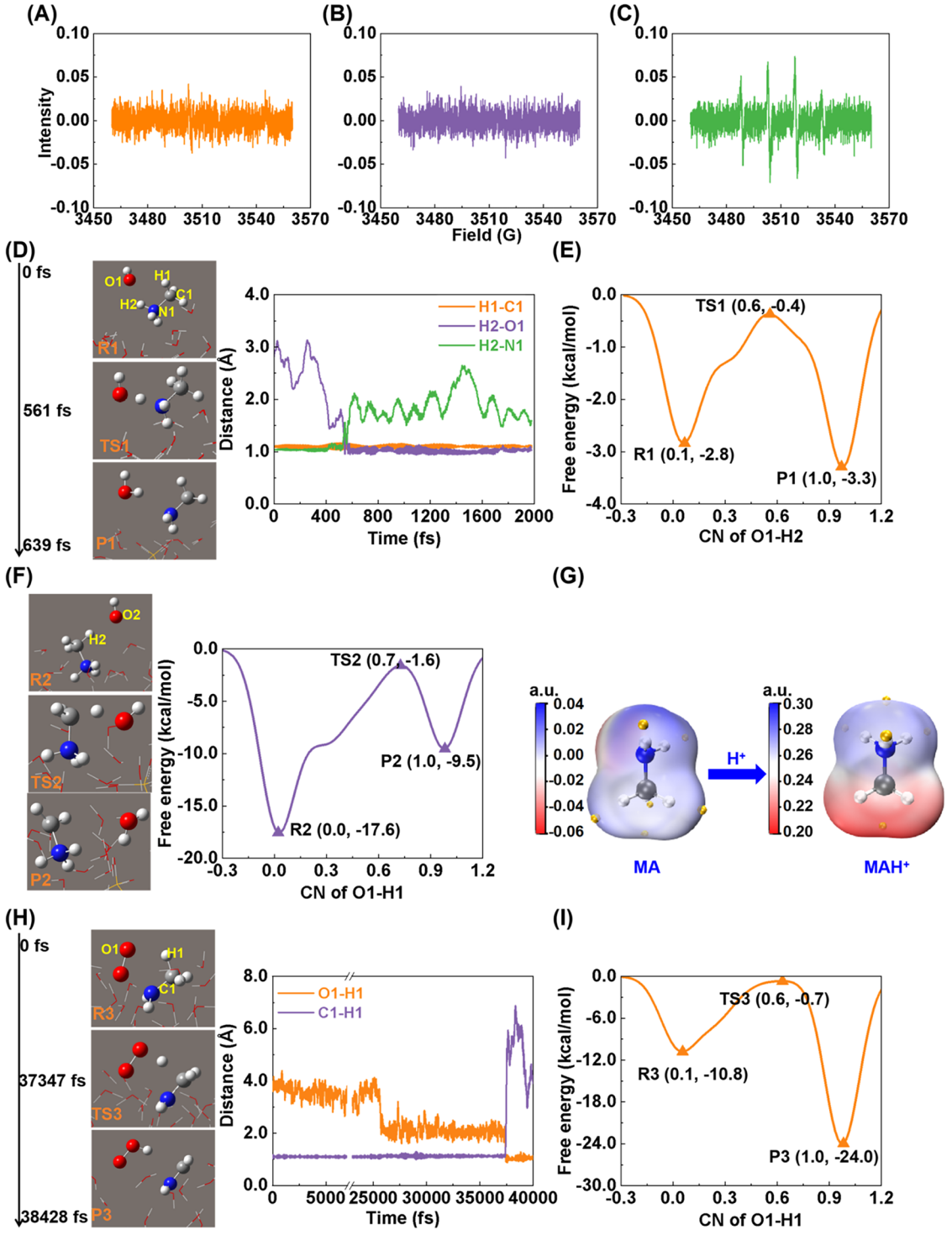

Figure 1. $^{\bullet}$OH-initiated oxidation of $NH_3CH_3^+$. EPR spectra of ultrasonic sulfate at pH ∼ 5 under conditions of: (A) in the dark without H_2O_2, (B) under natural light without H_2O_2 and (C) under natural light with H_2O_2. Oxidation of $NH_3CH_3^+$ by $^{\bullet}$OH: (D) key distance evolution and free energy distributions along paths of: (E) $^{\bullet}NH_2CH_3^+$ formation and (F) $NH_3CH_2^{+\bullet}$ formation. (G) The change in the electrostatic potential energy surface before and after methylamine protonation, where the yellow ball represents the maximum point of the electrostatic potential. O_2-addition reaction of $^{\bullet}NH_2CH_3^+$: (H) key distance evolution, and (I) free energy distribution along the path of $NH_2CH_2^{+\bullet}$ formation. R, TS, and P indicate the reaction reactant, transition state, and product, respectively. Key evolutions are determined via BOMD calculations, and free energy distributions are calculated via MTD calculations.

This suggests that amine ions are more chemically stable than amine molecules under ambient conditions. Therefore, we speculate that other active species should participate in and activate the ozonation reactivity of amine salts in fine PM.

Sulfate (HSO_4^-/SO_4^{2-}) is the dominant inorganic component in ultrafine/fine PM,[31,32] contributing to PM masses greater than 40% in several areas.[33] Previous experimental studies have shown that HSO_4^- is converted into sulfate radical anions ($SO_4^{\bullet-}$) by $^{\bullet}$OH-initiated oxidation, accounting for

https://doi.org/10.1021/jacs.5c04343
J. Am. Chem. Soc. 2025, 147, 34327−34338

organic compound oxidation in the aqueous phase.[34,35] Therefore, a sufficient HSO_4^- concentration is essential for $SO_4^{\bullet-}$ generation, although this is not reported in these experiments. This might work for aqueous PM with strong acidity (pH = 0−2),[36] for which the HSO_4^- concentration fraction is equal to that of SO_4^{2-}. However, for aqueous fine PM with weak acidity (pH = 4−6), the HSO_4^- concentration fraction dramatically decreases to 0, as determined by the acid−base equilibrium of the HSO_4^-/SO_4^{2-} system.[37] In particular, fine PM with pH = 4−6 is ubiquitous at the global scale,[38] where the HSO_4^- concentration is extremely low; rather, SO_4^{2-} contributes the most to fine PM. Therefore, $SO_4^{\bullet-}$ generation from HSO_4^- oxidation is very limited in atmospheric fine PM, which cannot account for amine salt ozonation activation. Additionally, recent studies state that organic compound oxidation could be initiated by $SO_4^{\bullet-}$ derived from ultraviolet light irradiation of SO_4^{2-} in aqueous fine PM.[39] However, our electron paramagnetic resonance (EPR) spectroscopy results indicate that no $SO_4^{\bullet-}$ is formed under natural light (Figure 1A,B). By contrast, when $^{\bullet}OH$ is introduced into SO_4^{2-} solution, strong signals of oxidant products from amine salt are detected via proton-transfer-reaction time-of-flight mass spectrometer (PTR-TOF-MS, in Figure S1). This confirms that amine salt ozonation cannot be initiated by a single SO_4^{2-} under natural light. Therefore, $^{\bullet}OH$ is speculated to function in activating the ozonation of amine salts.

In this study, ab initio calculations, PTR-TOF-MS, PTR-quadrupole mass spectrometry (PTR-QMS) and EPR methods are combined to systematically investigate the ozonation activation mechanism of methylamine salt (proxy amine salt) in aqueous sulfate PM (In theoretical calculations, a sphere model containing sulfate ions, methylamine ions and water molecules is used to represent sulfate PM; in experiments, a sulfate-containing solution is used to represent sulfate PM). On the basis of new data, we propose the sulfate-dominant ozonation mechanism of amine salts, which is proposed to be a potentially important mechanism of amine loss in the atmosphere. Herein, gaseous $^{\bullet}OH$, rather than $SO_4^{\bullet-}$, acts as an oxidant to initiate methylamine salt ions under natural light. Moreover, SO_4^{2-} activates methylamine salt ozonation reactivity and accelerates subsequent ozonation. Moreover, this is shown to be unique for sulfate, and is not feasible for chloride or nitrate anions in fine PM. To our knowledge, this ozonation mechanism of amine salts is novel and needs to be invoked in fine PM chemistry.

2. METHODS

2.1. Theoretical Calculations. Born−Oppenheimer molecular dynamics (BOMD) and metadynamics (MTD) simulations are implemented in the CP2K package[40,41] to explore the ozonation process of methylamine ions ($NH_3CH_3^+$) in fine PM. As shown in Figure S2, the simulation uses a spherical model containing sulfate ions, methylamine ions and water molecules to represent sulfate PM, where the white balls represent H, blue balls represent N, gray balls represent C, red balls represent O, and yellow balls represent S. The Becke−Lee−Yang−Parr exchange−correlation functional[42,43] with Grimme's dispersion correction (BLYP-D3) is used.[44−46] The valence and core electrons are treated with double-ζ + polarization DV2P basis sets[47] and Goedecker−Teter−Hutter (GTH) norm-conserving pseudopotentials,[48,49] respectively. Before all the simulations, to achieve the equilibrium state, the system undergoes geometry optimization in the NVT ensemble for 10,000 steps. Here, N, V, and T represent the number of atoms, volume, and temperature, respectively. The calculated reaction barrier ($\Delta G^{\ddagger}$) and reaction rate constant (k) are summarized in Supporting Information (SI), Tables S1 and S2.

2.2. Mass Spectrometry Experiments. To verify the proposed activation mechanism of methylamine cation oxidation, as shown in Figure S3, six groups of experiments are designed using a sulfate-containing solution to represent sulfate PM, and the concentration of the corresponding products in the headspace of the volumetric flask are quantitatively detected. Each experiment involves the addition of equimolar amounts of methylamine (MA) and hydrochloric acid (HCl) to ensure complete protonation of the MA in solution. The pH of each group of experimental solutions is controlled between 4 and 6 to ensure compliance with the true atmospheric fine PM acidity.[38] First, a set of pre-experiment is performed before the formal experiment to detect formaldehyde (HCHO) and hydrogen cyanide (HCN) by using PTR-TOF-MS-1000 (Ionicon Analytik, Innsbruck, Austria). Furthermore, HCHO and HCN's concentrations are measured via PTR-QMS-300 (Ionicon Analytik, Innsbruck, Austria). The measurement principles and technical details of the PTR-QMS and PTR-TOF-MS are extensively described in previous literature.[50−52]

2.3. EPR Experiments. The presence of free radicals in the dark without $^{\bullet}OH$, under natural light without $^{\bullet}OH$, and under natural light with $^{\bullet}OH$ is also confirmed via EPR. All the configured solutions remain at pH ∼ 5 and contain a circular nitro spin trap 5,5-dimethyl-1-pyrroliin-*N*-oxide (DMPO) for O-center radical trapping. More computational and experimental details are provided in Part 1 of the Supporting Information (SI).

3. RESULTS AND DISCUSSION

3.1. Ozonation Activation Mechanism. Previous studies have suggested that $^{\bullet}OH$ can oxidize HSO_4^- to form $SO_4^{\bullet-}$[39] or oxidize SO_4^{2-} under the catalysis of iron oxide to form $SO_4^{\bullet-}$[53] and that $SO_4^{\bullet-}$ may be able to oxidize $NH_3CH_3^+$. Therefore, the same sulfate solutions under three conditions—in the dark without H_2O_2, under natural light without H_2O_2, and under natural light with H_2O_2—are detected by EPR. As shown in Figure 1, no $SO_4^{\bullet-}$ signal is detected in any of the samples, and only the $^{\bullet}OH$ signal is detected in the sample with H_2O_2 (Figure 1C). Therefore, we speculate that $NH_3CH_3^+$ should be initially oxidized by $^{\bullet}OH$ rather than $SO_4^{\bullet-}$ in fine PM under natural light.

For further verification, five separate BOMD simulations are carried out to simulate the reaction of $NH_3CH_3^+$ with $^{\bullet}OH$ in sulfate aerosols. Similar to the reactions of methylamine molecules (NH_2CH_3) with $^{\bullet}OH$,[54,55] N-centered radicals ($^{\bullet}NH_2CH_3^+$, reaction 1) and C-centered radicals ($NH_3CH_2^{+\bullet}$, reaction 2) might be produced.

$$NH_3CH_3^+ + {}^{\bullet}OH \rightarrow {}^{\bullet}NH_2CH_3^+ + H_2O \quad (1)$$

$$NH_3CH_3^+ + {}^{\bullet}OH \rightarrow {}^{\bullet}NH_3CH_2^+ + H_2O \quad (2)$$

Unexpectedly, only $^{\bullet}NH_2CH_3^+$ is confirmed in the five independent BOMD simulations (Figures 1D and S4). MTD calculations are carried out to provide thermodynamic and kinetic evidence. The $\Delta G^{\ddagger}$ value of the $^{\bullet}NH_2CH_3^+$ formation path is calculated as 2.4 kcal/mol (Figure 1E), and k is 1.08×10^{11} $M^{-1}s^{-1}$. For the $NH_3CH_2^{+\bullet}$ formation path, k is 1.15×10 $M^{-1}s^{-1}$, as determined by $\Delta G^{\ddagger}$ = 16 kcal/mol (Figure 1F). Taken together, the branching ratio of $^{\bullet}NH_2CH_3^+$ formation path is 100%, indicating that $^{\bullet}NH_2CH_3^+$ is the dominant intermediate from the initial oxidation of $NH_3CH_3^+$ by $^{\bullet}OH$, and the total k is 1.08×10^{11} $M^{-1}s^{-1}$. $^{\bullet}NH_2CH_3^+$ subsequently carries out O_2- addition (reaction 3).

$$ {}^{\bullet}NH_2CH_3^+ + O_2 \rightarrow NH_2CH_2^+ + {}^{\bullet}HO_2 \quad (3)$$

https://doi.org/10.1021/jacs.5c04343
J. Am. Chem. Soc. 2025, 147, 34327−34338

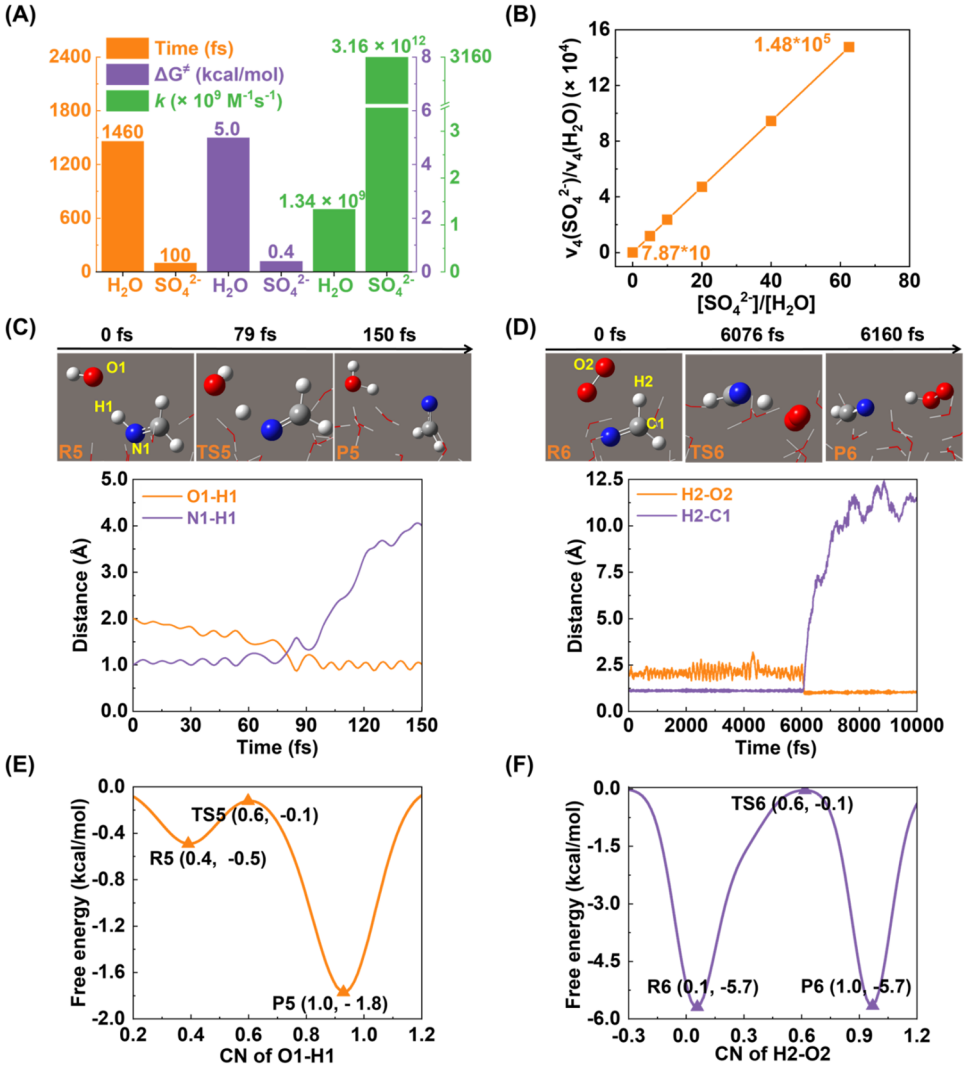

Figure 2. Formation and oxidation reactions of the $NHCH_2$ intermediate. (A) The reaction time, $\Delta G^{\ddagger}$ and k, of $NHCH_2$ formation from $NH_2CH_2^+$ deprotonation by H_2O/SO_4^{2-}. The reaction time and $\Delta G^{\ddagger}$ are calculated on the basis of the BOMD and MTD results in the Figure S6. (B) Changes in the $NHCH_2$ yield rate $v_4(SO_4^{2-})/v_4(H_2O)$ with the concentration ratio $[SO_4^{2-}]/[H_2O]$ in fine PM. Oxidation reaction of $NHCH_2$ with $^{\bullet}OH$ and O_2: (C, D) key distance evolution and (E, F) free energy distributions. R, TS, and P indicate the reaction reactant, transition state, and product, respectively. Key evolutions are determined via BOMD calculations, and free energy distributions are calculated via MTD calculations.

The BOMD trajectory shows that a complex of $^{\bullet}NH_2CH_3^+\cdots O_2$ with a lifetime of 12000 fs is formed (Figure 1H), which is not found in the gaseous oxidation of NH_2CH_3 molecules.[56] At t = 37,428 fs, a methylimine ion ($NH_2CH_2^+$) is formed, overcoming a $\Delta G^{\ddagger}$ of 10.1 kcal/mol (Figure 1I). The above results explain why the oxidation reactivity of $NH_3CH_3^+$ is completely different from that of NH_2CH_3.

To explain the intrinsic reactivity differences between $NH_3CH_3^+$ ion and the NH_2CH_3 molecule, the related electrostatic potential energy surface of $NH_3CH_3^+$ ion is compared to that of NH_2CH_3 molecule. As shown in Figure 1G, the electrostatic potential maxima of NH_2CH_3 molecules are uniformly distributed on H_C (the hydrogen of the methyl $-CH_3$ group) and H_N (the hydrogen of $-NH_2$ group). This illustrates why H_N and H_C can be abstracted by $^{\bullet}OH$ in almost equal chances, resulting in $^{\bullet}NH_2CH_3$ and $NH_3CH_2^{\bullet}$ formation from NH_2CH_3 molecule.[57,58] For $NH_3CH_3^+$ ions, the electrostatic potential maxima points are focused mainly on H_N. This finding indicates that only H_N-abstraction by $^{\bullet}OH$ is feasible and generates $^{\bullet}NH_2CH_3^+$, which is consistent with previous studies showing that the protonation of N atoms inhibits H extraction at the α-C position.[59,60]

Although our results have confirmed that $SO_4^{\bullet-}$ cannot be formed under natural light (Figure 1), we still discuss the competition reactions between $NH_3CH_3^+$ oxidation by $^{\bullet}OH$ and $SO_4^{\bullet-}$. On the basis of our MTD results for $NH_3CH_3^+$ by $SO_4^{\bullet-}$ (Figure S5A), $\Delta G^{\ddagger}$ is calculated as 17.7 kcal/mol, and k is 6.49×10^{-1} $M^{-1}s^{-1}$. Therefore, the yield rate $v_1(SO_4^{\bullet-})$ of $^{\bullet}NH_2CH_3^+$ from $SO_4^{\bullet-}$-initiated oxidation is described as 6.49×10^{-1} $[NH_3CH_3^+] \times [SO_4^{\bullet-}]$ $M^{-1}s^{-1}$. On the basis of the present results, the yield rate $v_1(^{\bullet}OH)$ of $^{\bullet}NH_2CH_3^+$ from $^{\bullet}OH$-initiated oxidation is described as 1.08×10^{11} $[NH_3CH_3^+] \times [^{\bullet}OH]$ $M^{-1}s^{-1}$. Accordingly, the competitive ratio $v_1(^{\bullet}OH)/v_1(SO_4^{\bullet-})$ in aerosols is denoted as 1.66×10^{11} $[^{\bullet}OH]/[SO_4^{\bullet-}]$. For atmospheric aerosols, the mean value of $[^{\bullet}OH]$ is 1.81×10^{-15} M,[61] and that of $[SO_4^{\bullet-}]$ is 1.00×10^{-14}–3.00×10^{-14} M.[39] Thus, the ratio $v_1(^{\bullet}OH)/v_1(SO_4^{\bullet-})$ is calculated as 1.00×10^{10}–3.01×10^{10} under ambient conditions (Figure S5B), implying that $^{\bullet}OH$ plays a dominant role in the initial oxidation of $NH_3CH_3^+$ in universal fine PM even when $SO_4^{\bullet-}$ exists.

https://doi.org/10.1021/jacs.5c04343
J. Am. Chem. Soc. 2025, 147, 34327−34338

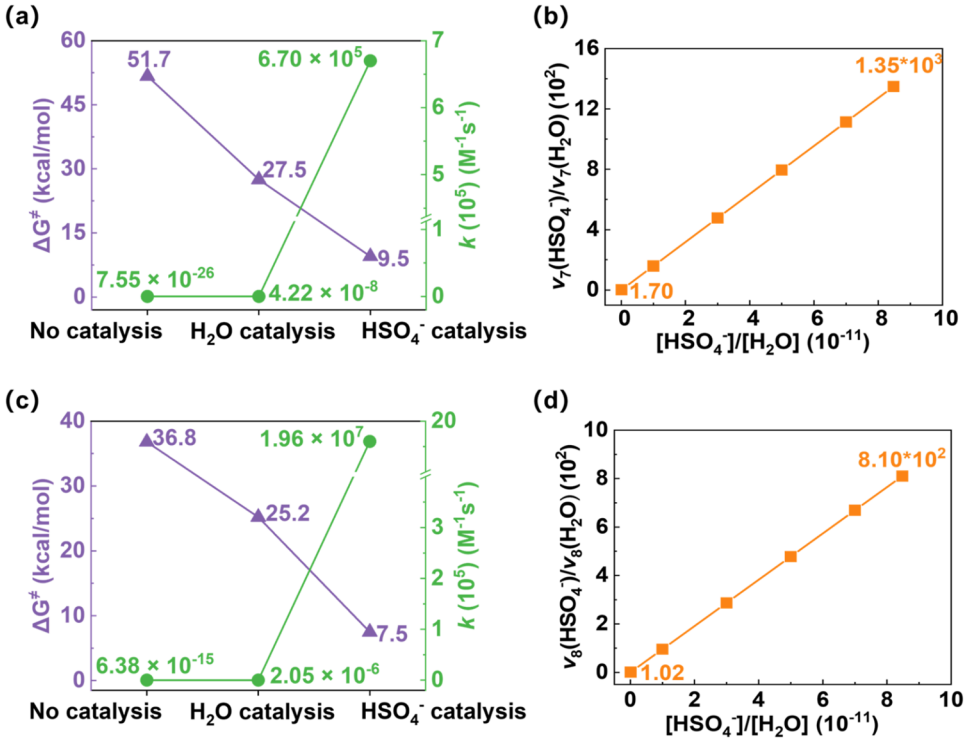

Figure 3. Formation and decomposition of the NH_2CH_2OH intermediate under no catalysis, H_2O catalysis and HSO_4^- catalysis, respectively. (A) $\Delta G^{\ddagger}$ and k values of NH_2CH_2OH formation. (B) Changes in the NH_2CH_2OH formation rate $v_7(HSO_4^-)/v_7(H_2O)$ with the concentration ratio $[HSO_4^-]/[H_2O]$ in fine PM. (C) $\Delta G^{\ddagger}$ and k values of NH_2CH_2OH decomposition. (D) Change in the NH_2CH_2OH decomposition rate $v_8(HSO_4^-)/v_8(H_2O)$ with the concentration ratio $[HSO_4^-]/[H_2O]$. All the $\Delta G^{\ddagger}$ and k values are calculated on the basis of the MTD results in the Figure S7.

Considering the components of fine PM, $NH_2CH_2^+$ could be further deprotonated by SO_4^{2-} or H_2O (reaction 4).

$$NH_2CH_2^+ + SO_4^{2-}/H_2O \rightarrow NHCH_2 + HSO_4^-/H_3O^+ \quad (4)$$

The product methylenimine molecule ($NHCH_2$), which is the intermediate of methylamine salt ozonation, has ozonation activity.[62,63] Based on the present BOMD simulation (Figure S6A,C), the deprotonation times of the two methods are compared in Figure 2A. For deprotonation by H_2O, $NH_2CH_2^+$ first forms a stable complex of $NHCH_2\cdots H_2O$ at 360 fs and then converts to $NHCH_2$ after 1100 fs. In contrast, the deprotonation time of SO_4^{2-} is approximately 10% (100 fs) greater than that of H_2O, implying faster $NHCH_2$ generation. Moreover, MTD simulations (Figure S6B,D) and kinetics calculations provide more details about their competitiveness. The related $\Delta G^{\ddagger}$ value of deprotonation by H_2O is 5.0 kcal/mol, and k is 1.34×10^9 $M^{-1}s^{-1}$. Accordingly, the $NHCH_2$ yield rate $v_4(H_2O)$ is denoted as 1.34×10^9 $[NH_2CH_2^+] \times [H_2O]$ $M^{-1}s^{-1}$. In contrast, the $\Delta G^{\ddagger}$ of deprotonation by SO_4^{2-} is only 0.4 kcal/mol, which is less than 10% of that of deprotonation by H_2O. The derived k value is 3.16×10^{12} $M^{-1}s^{-1}$, indicating that $NHCH_2$ yield rate $v_4(SO_4^{2-})$ is 3.16×10^{12} $[NH_2CH_2^+] \times [SO_4^{2-}]$ $M^{-1}s^{-1}$. Therefore, the complete ratio $v_4(SO_4^{2-})/v_4(H_2O)$ is denoted as 2.36×10^{12} $[SO_4^{2-}]/[H_2O]$, which is displayed in Figure 2B. For atmospheric fine PM, $[H_2O]$ varies from 1.2 to 89.9 $\mu g/m^3$,[64] and $[SO_4^{2-}]$ varies from 3.0 to 75.0 $\mu g/m^3$.[65] Accordingly, the real $NHCH_2$ yield rate ratio of $v_4(SO_4^{2-})/v_4(H_2O)$ is calculated as 7.88×10^{10}–1.48×10^{14}, implying that SO_4^{2-}, rather than H_2O, plays a dominant role in accelerating the yields of $NHCH_2$ intermediate in atmospheric fine PM.

However, $NHCH_2$ is chemically unstable and can be rapidly converted into HCN through an oxidation reaction with $^{\bullet}OH$/O_2 in gas phase.[62,66] Gas-phase radicals, especially $^{\bullet}OH$, play a significant role in the degradation of organic matter.[67,68] Therefore, we further investigate the feasibility of $NHCH_2$ reaction with $^{\bullet}OH/O_2$ in fine PM (from reactions 5 to 6).

$$NHCH_2 + {}^{\bullet}OH \rightarrow {}^{\bullet}NCH_2 + H_2O \quad (5)$$

$$^{\bullet}NCH_2 + O_2 \rightarrow HCN + {}^{\bullet}HO_2 \quad (6)$$

The BOMD results show that the first H-abstraction step by $^{\bullet}OH$ (reaction 5) occurs within 79 fs (Figure 2C), and the second H-abstraction step by O_2 (reaction 6) occurs within 6076 fs (Figure 2D). Clearly, the second H-abstraction step is the rate-limiting step. The MTD results (Figure 2E,F) reveal that the $\Delta G^{\ddagger}$ values of these two H-abstraction steps are 0.4 and 5.6 kcal/mol, and the corresponding k values are 3.16×10^{12} and 4.86×10^8 $M^{-1}s^{-1}$, respectively. Therefore, consistent with the BOMD results, the second H-abstraction step is the decisive step of $NHCH_2$ oxidation, and the total k is 4.86×10^8 $M^{-1}s^{-1}$. Compared with 3.0×10^{-12}–1.7×10^{-11} $M^{-1}s^{-1}$ in gas phase,[62,66] $NHCH_2$ conversion into HCN in fine PM is promoted by 19–20 orders of magnitude. The difference in k values between the two phases is induced by surface solvation effect.

Moreover, $NHCH_2$ is supposed to readily carry out hydration reactions, converting into aminomethanol (NH_2CH_2OH) in fine PM (reaction 7).[69,70]

$$NHCH_2 + H_2O \rightarrow NH_2CH_2OH \quad (7)$$

The product NH_2CH_2OH can undergo ozonation,[63] which has been confirmed as an intermediate in methylamine salt ozonation. However, on the basis of our MTD results (Figures 3

https://doi.org/10.1021/jacs.5c04343
J. Am. Chem. Soc. 2025, 147, 34327−34338

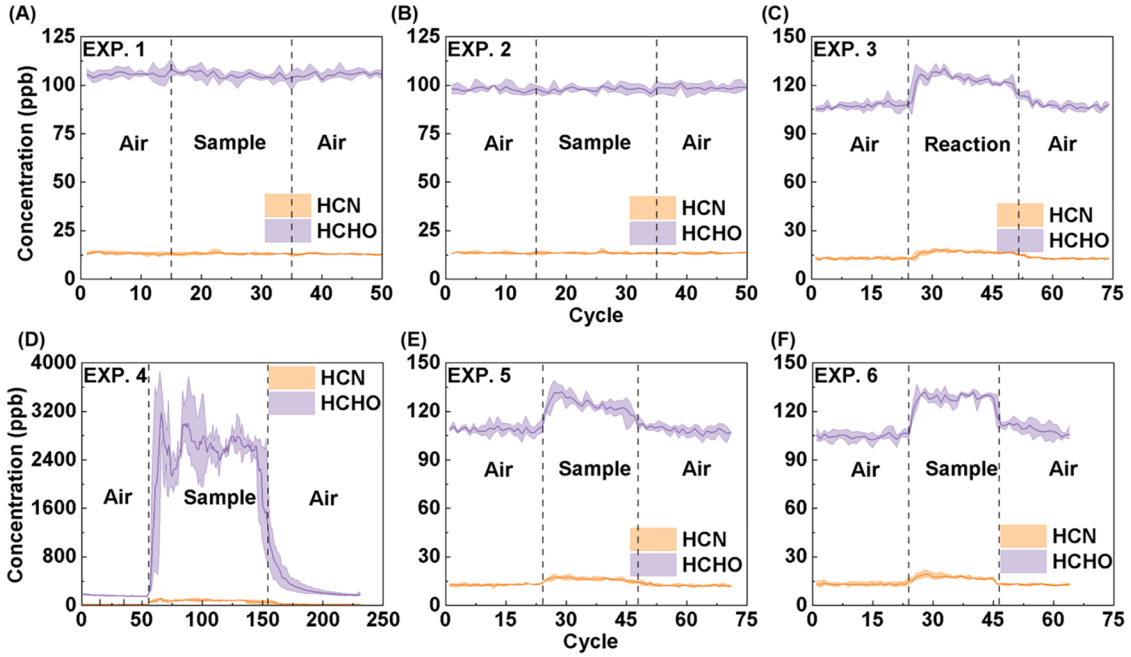

Figure 4. $NHCH_2$ and NH_2CH_2OH formation confirmed by PTR-QMS. Changes in the concentrations of HCHO and HCN detected in EXPs. 1−6, respectively. The six EXPs are carried out (A) without $^{\bullet}OH$ and without any ions (Table S3, EXP. 1), (B) without $^{\bullet}OH$ and with SO_4^{2-} (Table S3, EXP. 2), (C) with $^{\bullet}OH$ and without any ions (Table S3, EXP. 3), (D) with $^{\bullet}OH$ and with SO_4^{2-} (Table S3, EXP. 4), (E) with $^{\bullet}OH$ and with Cl^- (Table S3, EXP. 5), and (F) with $^{\bullet}OH$ and with NO_3^- (Table S3, EXP. 6).

and S7), the $\Delta G^{\ddagger}$ value of direct hydration is calculated as 51.7 kcal/mol, and the related k is as low as 7.55×10^{-26} $M^{-1}s^{-1}$, which cannot explain rapid hydration reaction of $NHCH_2$ in fine PM. Water is found to act as a positive catalyst in many heterogeneous reactions.[71−73] Our results show that this is also true in $NHCH_2$ hydration reaction in fine PM. The MTD results show that under water catalysis, the related $\Delta G^{\ddagger}$ decreases to 27.5 kcal/mol, and k increases to 4.22×10^{-8} $M^{-1}s^{-1}$, indicating a promoting effect on the hydration reaction. In addition, HSO_4^- is common in regular fine PM and is also a byproduct of $NH_2CH_2^+$ deprotonation by SO_4^{2-}. Hence, we further investigated HSO_4^- catalysis of $NHCH_2$ hydration reaction. Present results display that the corresponding $\Delta G^{\ddagger}$ value significantly decreases to 9.5 kcal/mol and that k dramatically increases to 6.70×10^5 $M^{-1}s^{-1}$. Therefore, both H_2O and HSO_4^- promote $NHCH_2$ hydration in atmospheric sulfate fine PM. To further determine which factor plays a leading role in promoting $NHCH_2$ hydration, the ratio $v_7(HSO_4^-)/v_7(H_2O)$ is calculated as a function of $[HSO_4^-]/[H_2O]$, where $v_7(H_2O)$ and $v_7(HSO_4^-)$ represent the NH_2CH_2OH yield rates caused by H_2O and HSO_4^-, respectively. For atmospheric fine PM, $[HSO_4^-]/[H_2O]$ equals 1.07×10^{-13}−8.48×10^{-11}.[64,74] Thus, as shown in Figure 3B, $v_7(HSO_4^-)/v_7(H_2O)$ is calculated as 1.70−1.35×10^3 in fine PM. This implies that HSO_4^-, rather than water, significantly accelerates NH_2CH_2OH intermediate of methylamine salt ozonation in regular fine PM.

NH_2CH_2OH is reported to be unstable[75] and can be decomposed into HCHO and ammonia (NH_3).[76−78] In addition to promoting $NHCH_2$ hydration, H_2O and HSO_4^- strongly accelerate NH_2CH_2OH decomposition (reaction 8).

$$NH_2CH_2OH \rightarrow HCHO + NH_3 \quad (8)$$

Based on our MTD results (Figure 3C), the $\Delta G^{\ddagger}$ value of direct decomposition is 36.8 kcal/mol, and the derived k is 6.38×10^{-15} s^{-1}, implying a difficult reaction under ambient conditions. In contrast, the related $\Delta G^{\ddagger}$ value decreases to 25.2 kcal/mol because of H_2O catalysis and to 7.5 kcal/mol because of HSO_4^- catalysis. The derived k increases to 2.05×10^{-6} s^{-1} for the former and 1.96×10^7 s^{-1} for the latter. Clearly, NH_2CH_2OH decomposition is greatly promoted in regular sulfate fine PM. The ratio $v_8(HSO_4^-)/v_8(H_2O)$ is thus determined by $[HSO_4^-]/[H_2O]$, where $v_8(H_2O)$ and $v_8(HSO_4^-)$ represent NH_2CH_2OH decomposition rates caused by H_2O and HSO_4^-, respectively. As shown in Figure 3D, the real HCHO and NH_3 yield ratio of $v_8(HSO_4^-)/v_8(H_2O)$ is calculated as 1.02−8.10×10^2 under ambient conditions. Therefore, similar circumstances are confirmed for $NHCH_2$ hydration, and HSO_4^- also plays a role in accelerating NH_2CH_2OH decomposition in regular fine PM.

3.2. Verified by Mass Spectrometry. To verify the proposed ozonation activation mechanism, PTR-TOF-MS is applied to confirm the formations of HCHO and HCN, and the related concentrations are measured by using PTR-QMS. The different experimental conditions and calculated average concentrations of each product are summarized in Table S3. The corresponding detected concentration profiles are in Figure 4. The Exp. One result shows that neither [HCHO] nor [HCN] increases (Figure 4A) without $^{\bullet}OH$ or SO_4^{2-}. Moreover, the Exp. Two results reveal the same phenomenon when SO_4^{2-} is added (Figure 4B). Exp. One and Exp. Two together indicate that $NHCH_2$ is not formed without $^{\bullet}OH$-initiated oxidation. In contrast, $NHCH_2$ is formed after H_2O_2 is added in Exp. Three (Figure 4C), which is indicated by the significant growth of [HCHO] and [HCN]. This state of $^{\bullet}OH$-initiated oxidation is really required to activate $NH_3CH_3^+$.

$NH_2CH_2^+$ deprotonation reaction is caused predominantly by SO_4^{2-} in our proposed activation mechanism, which is the second requirement for $NH_3CH_3^+$ activation. To verify this, SO_4^{2-} is added in Exp. 4 on the basis of Exp. 3. As expected, [HCHO] and [HCN] in Exp. 4 (Figure 4D) dramatically

https://doi.org/10.1021/jacs.5c04343
J. Am. Chem. Soc. 2025, 147, 34327−34338

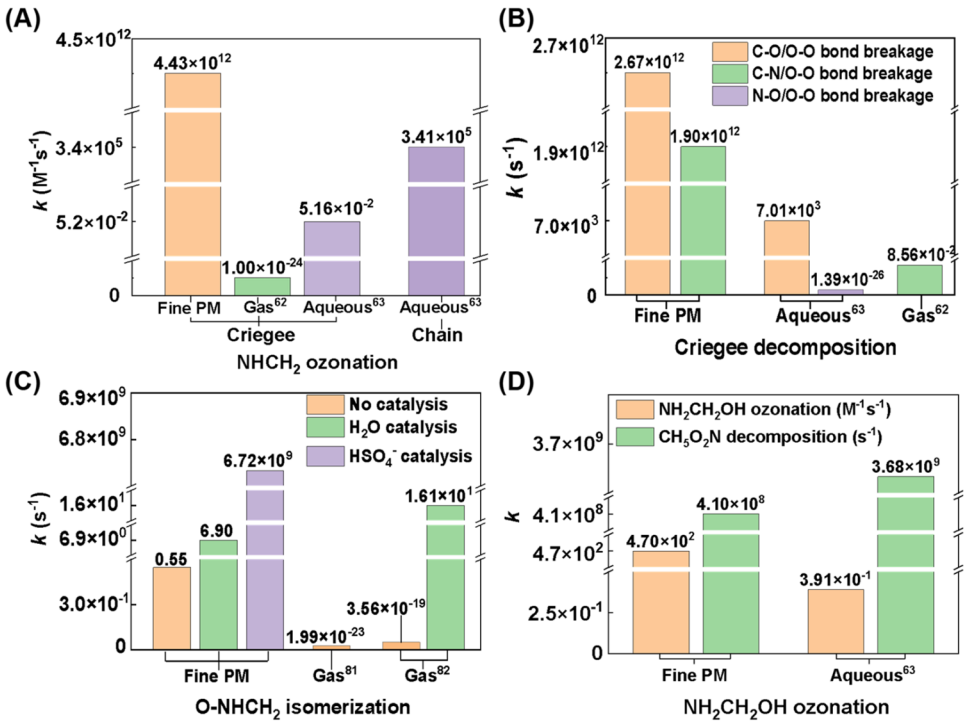

Figure 5. k of the subsequent ozonation reactions for $NHCH_2$ and NH_2CH_2OH in the fine PM, gas and aqueous phases, respectively. (A) $NHCH_2$ ozonation through the Criegee and chain paths. (B) Criegee intermediate decomposition. (C) O-$NHCH_2$ isomerization under different catalytic effects. (D) NH_2CH_2OH ozonation. k of fine PM in this work is calculated on the basis of the MTD results in the Figures S8 and S9, and k in the gas and aqueous phases are obtained from the literature.

increase by 1 order of magnitude compared with those in Exp. 3. This finding illustrates that SO_4^{2-} significantly enhances methylamine ion deprotonation, which is consistent with our theoretical calculation results.

However, in Exp. 3, $NH_2CH_2^+$ deprotonation might have been caused by Cl^-. To determine whether Cl^- could cause $NH_2CH_2^+$ deprotonation, more Cl^- is added in Exp. 5 than in Exp. 3. As shown in Exp. 5 (Figure 4E), [HCHO] and [HCN] remain equal to those observed in Exp. 3 (Figure 4C), indicating that water, rather than Cl^-, contributes to $NH_2CH_2^+$ deprotonation. Similarly, we also examine whether NO_3^- can cause this deprotonation. For this purpose, NO_3^- is added in Exp. 6 on the basis of Exp. 3. Similar to Exp. 5, neither [HCHO] nor [HCN] in Exp. 6 (Figure 4F) further increases based on those observed in Exp. 3. Therefore, NO_3^- cannot lead to $NH_2CH_2^+$ deprotonation. Taken together, these results indicate that, in nitrate or chlorine salt PM, $NH_2CH_2^+$ ozonation activation relies only on the water content but not inorganic ions (Cl^- and NO_3^-). Moreover, owing to SO_4^{2-} enhancement of $NH_2CH_2^+$ deprotonation, $NH_2CH_2^+$ ozonation activation is expected to be more rapid in sulfate aerosols than in nitrate or chlorine salt aerosols under the same atmospheric conditions.

3.3. Subsequent Ozonation. For two intermediates ($NHCH_2$ and NH_2CH_2OH), we further investigated their ozonation mechanisms in fine PM. The corresponding energy barriers are calculated (Figures S8 and S9). Rate constants are thus determined and compared to those in gas phase or aqueous phase.[62,63] Some new findings are found here (Figure 5). For $NHCH_2$ ozonation in aqueous phase, the dominant product is formamide (NH_2CHO) produced from the chain path (from reactions 9 to 10),[63] whereas for fine PM particles, the dominant product is changed to formaldonitrone (O-$NHCH_2$) yielded from the Criegee path (from reactions 11 to 13 and Figure S8A).

$$\text{Chain reaction: } NHCH_2 + O_3 \rightarrow NHCH_2O_3 \quad (9)$$

$$NHCH_2O_3 \rightarrow O{=}CHNH_2 + O_2 \quad (10)$$

$$\text{Crigee reaction: } NHCH_2 + O_3 \rightarrow NHCH_2O_3 \quad (11)$$

$$NHCH_2O_3 \rightarrow HCHO + HNOO \quad (12)$$

$$NHCH_2O_3 \rightarrow O\text{-}NHCH_2 + O_2 \quad (13)$$

This can be caused by the lower density of water molecules at the air−water interface, positioning the C═N bond favorably for reacting with gas−phase molecules, thereby increasing the likelihood of the Criegee path.[79,80] Moreover, in previous studies, it was reported that $NHCH_2$ undergoes a Criegee reaction with a small k of 1.0×10^{-24} $M^{-1}s^{-1}$ in gas phase,[62] whereas the present results revealed that k (4.43×10^{12} $M^{-1}s^{-1}$) is dramatically increased by 36 orders of magnitude in fine PM (Figure 5A). Moreover, the decomposition of the produced Criegee intermediate (Figure 5B) is also accelerated in reaction 12 (C−O/O−O bond breakage) and reaction 13 (N−C/O−O bond breakage). The related k value is 2.67×10^{12} s^{-1} for the former and 1.90×10^{12} s^{-1} for the latter. Accordingly, the total k of decomposition is 4.57×10^{12} s^{-1} in fine PM, which is 14 orders of magnitude greater than that in gas phase[62] and 9 orders of magnitude greater than that in aqueous phase.[63] Afterward, formaldonitrone (O-$NHCH_2$) and formaldehyde (HCHO) are produced, which has also been observed in previous experimental studies.[11]

https://doi.org/10.1021/jacs.5c04343
J. Am. Chem. Soc. 2025, 147, 34327−34338

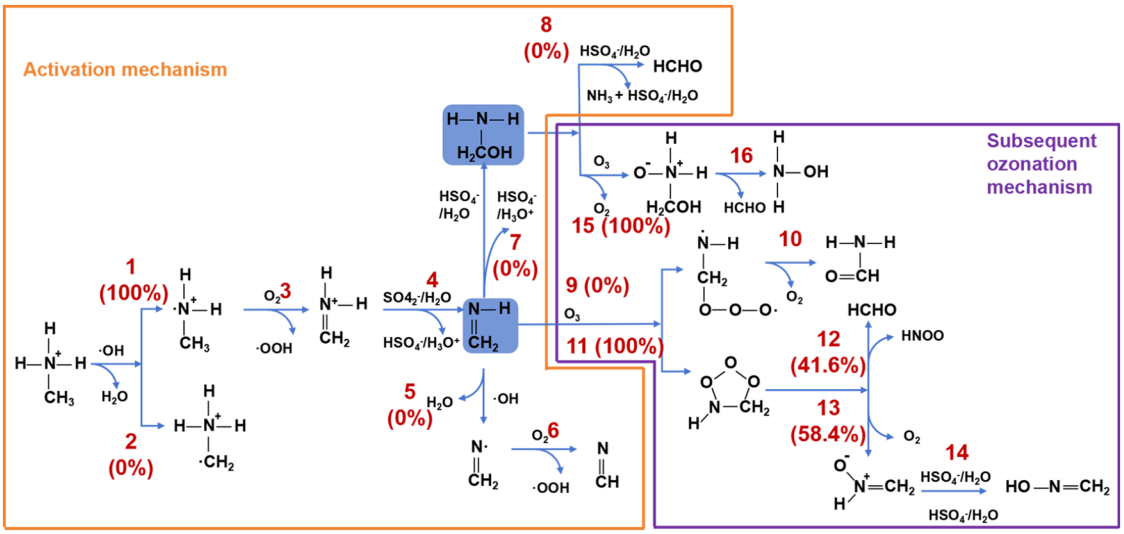

Figure 6. •OH-sulfate synergistic ozonation mechanism of methylamine salt.

$O\text{-}NHCH_2$ subsequently undergoes isomerization, producing formaldoxime ($HO\text{-}NCH_2$, reaction 14).

$$O\text{-}NHCH_2 \rightarrow HO\text{-}NCH_2 \quad (14)$$

The differences between the isomerization reactions are compared in gas phase and fine PM (Figure 5C). Previous studies have revealed that, in gas phase, $O\text{-}NHCH_2$ undergoes one-step isomerization with a small k value of 1.99×10^{-23}–3.56×10^{-19} s^{-1},[81,82] which rarely occurs under ambient conditions. The k value only increases to 1.61×10^{1} s^{-1} even under H_2O catalysis in gas phase.[82] In contrast, in fine PM, $O\text{-}NHCH_2$ undergoes rapid isomerization through two steps: $O\text{-}NHCH_2\cdots HSO_4^-$ complex formation and H-exchange by HSO_4^- (Figure S8E). Owing to this, $O\text{-}NHCH_2$ isomerization on fine PM surface is distinctly promoted. Specifically, (Figure S8F), under HSO_4^- catalysis, the higher $\Delta G^{\ddagger}$ value of the two-step is reduced to 3.9 kcal/mol, which is 12.4 kcal/mol lower than that (16.3 kcal/mol) under H_2O catalysis. This indicates that the total k value is increased to 6.72×10^{9} s^{-1} under HSO_4^- catalysis, which is 9 orders of magnitude greater than that (6.90 s^{-1}) under water catalysis. However, in atmospheric sulfate PM, the real $[HSO_4^-]/[H_2O]$ varies in the range of 1.07×10^{-13}–8.48×10^{-11}, and the isomerization rate ratio caused by HSO_4^- and water is calculated to be 1.42×10^{-3}–8.26×10^{-1}. Therefore, in atmospheric sulfate PM, HSO_4^- is found to assist water in promoting $O\text{-}NHCH_2$ isomerization. Importantly, our results clarify that oxime ($HO\text{-}NCH_2$) is the ozonation product of methylamine salt, which is mistakenly identified as an amide in experimental studies.[11]

The NH_2CH_2OH intermediate reacts with O_3 (reaction 15) and decomposes into HCHO and hydroxylamine (NH_2OH, reaction 16).

$$NH_2CH_2OH + O_3 \rightarrow CH_5O_2N + O_2 \quad (15)$$

$$CH_5O_2N \rightarrow NH_2OH + HCHO \quad (16)$$

Specifically, as shown in Figures 5D and S9A, O_3 directly attacks the N atom of NH_2CH_2OH, generating trans-CH_5O_2N and O_2 with $\Delta G^{\ddagger}$ of 13.8 kcal/mol and k of 4.70×10^{2} $M^{-1}s^{-1}$. Subsequently, trans-CH_5O_2N spontaneously converts to cis-CH_5O_2N (Figure S10) and decomposes into HCHO and NH_2OH, with a $\Delta G^{\ddagger}$ value of 5.7 kcal/mol and a k value of 4.10 $\times 10^{8}$ s^{-1}. The k values for these two steps are similar to those reported in previous studies (3.91×10^{-1}, 3.68×10^{9} $M^{-1}s^{-1}$).[63]

The complete ozonation mechanism is shown in Figure 6. The intermediate $NHCH_2$ is degraded through three pathways: oxidation with •OH (reaction 5), hydration with H_2O/HSO_4^- (reaction 7), and ozonation with O_3 (reaction 11). To verify the importance of the ozonation pathway, we calculated the branching ratios of the three pathways. The reaction rate v_{r7} for reaction 7 is calculated as 6.70×10^{5} $[NHCH_2] \times [H_2O] \times [HSO_4^-]$ $M^{-1}s^{-1}$. Average $[H_2O]$ is 2.53×10^{-9} M[64] and $[HSO_4^-]$ is 5.48×10^{-21} M[74] in universal aerosols. Thus, v_{r7} is calculated as $9.28 \times 10^{-24}[NHCH_2]$ s^{-1}. The reaction rate v_{r5} for reaction 5 is calculated as $3.16 \times 10^{12}[NHCH_2] \times [^{\bullet}OH]$ $M^{-1}s^{-1}$, the average $[^{\bullet}OH]$ is 1.81×10^{-15} M in atmosphere.[61] Accordingly, v_{r5} is calculated as $5.72 \times 10^{-3}[NHCH_2]$ s^{-1}. Similarly, the reaction rate v_{r11} for reaction 11 is calculated as $4.43 \times 10^{12}[NHCH_2] \times [O_3]$ $M^{-1}s^{-1}$. The average $[O_3]$ is 2.66×10^{-6} M in atmosphere.[83,84] Therefore, v_{r11} is calculated as $1.18 \times 10^{7}[NHCH_2]$ s^{-1}. Taken together, the branching ratio for reaction 11 is 100% under real atmospheric conditions. Likewise, we can also obtain that for all reaction paths involving NH_2CH_2OH, the branching ratio for reaction 15 with O_3 is 100%, too. In addition, many literatures have proved that there is a surface electric field in microdroplets, which can tear H_2O to produce •OH and promote the reaction,[85−87] and we do not consider the $[HSO_4^-]$ produced by the deprotonation of SO_4^{2-}, which means that the oxidation/hydration of $NHCH_2$ and the oxidation of $NH_3CH_3^+$ (reaction 1) are likely to become more feasible under real atmospheric conditions.

4. CONCLUSIONS

In this study, we find that inert methylamine ions can be activated through synergistic reactions of •OH-initiated oxidation and SO_4^{2-}-initiated deprotonation. The intermediate $NHCH_2$ is thus produced, and SO_4^{2-} accounts for its rapid formation. The NH_2CH_2OH intermediate is formed from $NHCH_2$ hydration and rapidly converts into HCHO, HCN and NH_3, and HSO_4^- is responsible for its rapid formation and conversion. This also explains why NH_2CH_2OH is undetected in experimental studies.[69,70] The subsequent ozonation of $NHCH_2$ and NH_2CH_2OH in sulfate PM is significantly

https://doi.org/10.1021/jacs.5c04343
J. Am. Chem. Soc. 2025, 147, 34327−34338

accelerated, leading to more rapid production of O-NHCH$_2$ and HCHO than in gas and aqueous phases.[62,63] HSO_4^- is found to assist water in promoting O-NHCH$_2$ isomerization in the HSO_4^- concentration range of real atmospheric PM. Notice that it cannot be directly speculated that NH=CH$_2$ is completely converted through reaction 11 (Figure 6) in the context of unknown kinetic rates in the ambient atmosphere. The 100% branching ratio through reaction 11 in this work is not absolute, and it is relative to reaction 9. Among the ozonation products we confirmed that aldehyde and hydroxylamine are consistent with the reported results of amine salt oxidation products in PM.[11] The findings from this work also clarify that oxime (formaldoxime, HO-NCH$_2$) is the ozonation product of the amine salt, which is mistaken for its isomeride amide in previous experimental studies.[11] Our findings deepen the understanding of the ozonations of amine salts in atmospheric fine PM.

■ ASSOCIATED CONTENT

Supporting Information

The Supporting Information is available free of charge at https://pubs.acs.org/doi/10.1021/jacs.5c04343.

Additional method details and supplementary figures, including computational details of the BOMD and MTD simulations, calculations of reaction rate constants and equilibrium constants, experimental details, Tables S1−S3 and Figures S1−S10 (PDF)

■ AUTHOR INFORMATION

Corresponding Author

Taicheng An − *Guangdong-Hong Kong-Macao Joint Laboratory for Contaminants Exposure and Health, Guangdong Key Laboratory of Environmental Catalysis and Health Risk Control, Institute of Environmental Health and Pollution Control, Guangdong University of Technology, Guangzhou 510006, China; Guangzhou Key Laboratory of Environmental Catalysis and Pollution Control, Key Laboratory for City Cluster Environmental Safety and Green Development of the Ministry of Education, School of Environmental Science and Engineering, Guangdong University of Technology, Guangzhou 510006, China*; Email: antc99@gdut.edu.cn

Authors

Weina Zhang − *Guangdong-Hong Kong-Macao Joint Laboratory for Contaminants Exposure and Health, Guangdong Key Laboratory of Environmental Catalysis and Health Risk Control, Institute of Environmental Health and Pollution Control, Guangdong University of Technology, Guangzhou 510006, China; Guangzhou Key Laboratory of Environmental Catalysis and Pollution Control, Key Laboratory for City Cluster Environmental Safety and Green Development of the Ministry of Education, School of Environmental Science and Engineering, Guangdong University of Technology, Guangzhou 510006, China*

Dayuan Zheng − *Guangdong-Hong Kong-Macao Joint Laboratory for Contaminants Exposure and Health, Guangdong Key Laboratory of Environmental Catalysis and Health Risk Control, Institute of Environmental Health and Pollution Control, Guangdong University of Technology, Guangzhou 510006, China; Guangzhou Key Laboratory of Environmental Catalysis and Pollution Control, Key Laboratory for City Cluster Environmental Safety and Green Development of the Ministry of Education, School of Environmental Science and Engineering, Guangdong University of Technology, Guangzhou 510006, China*

Jiale Lao − *Guangdong-Hong Kong-Macao Joint Laboratory for Contaminants Exposure and Health, Guangdong Key Laboratory of Environmental Catalysis and Health Risk Control, Institute of Environmental Health and Pollution Control, Guangdong University of Technology, Guangzhou 510006, China; Guangzhou Key Laboratory of Environmental Catalysis and Pollution Control, Key Laboratory for City Cluster Environmental Safety and Green Development of the Ministry of Education, School of Environmental Science and Engineering, Guangdong University of Technology, Guangzhou 510006, China*

Ruijing Li − *Guangdong-Hong Kong-Macao Joint Laboratory for Contaminants Exposure and Health, Guangdong Key Laboratory of Environmental Catalysis and Health Risk Control, Institute of Environmental Health and Pollution Control, Guangdong University of Technology, Guangzhou 510006, China; Guangzhou Key Laboratory of Environmental Catalysis and Pollution Control, Key Laboratory for City Cluster Environmental Safety and Green Development of the Ministry of Education, School of Environmental Science and Engineering, Guangdong University of Technology, Guangzhou 510006, China*

Baihang Chen − *Guangdong-Hong Kong-Macao Joint Laboratory for Contaminants Exposure and Health, Guangdong Key Laboratory of Environmental Catalysis and Health Risk Control, Institute of Environmental Health and Pollution Control, Guangdong University of Technology, Guangzhou 510006, China; Guangzhou Key Laboratory of Environmental Catalysis and Pollution Control, Key Laboratory for City Cluster Environmental Safety and Green Development of the Ministry of Education, School of Environmental Science and Engineering, Guangdong University of Technology, Guangzhou 510006, China*

Jiangyao Chen − *Guangdong-Hong Kong-Macao Joint Laboratory for Contaminants Exposure and Health, Guangdong Key Laboratory of Environmental Catalysis and Health Risk Control, Institute of Environmental Health and Pollution Control, Guangdong University of Technology, Guangzhou 510006, China; Guangzhou Key Laboratory of Environmental Catalysis and Pollution Control, Key Laboratory for City Cluster Environmental Safety and Green Development of the Ministry of Education, School of Environmental Science and Engineering, Guangdong University of Technology, Guangzhou 510006, China*; orcid.org/0000-0003-1491-2257

Jie Zhong − *School of Petroleum Engineering, China University of Petroleum (East China), Qingdao 266580, China*

Yuemeng Ji − *Guangdong-Hong Kong-Macao Joint Laboratory for Contaminants Exposure and Health, Guangdong Key Laboratory of Environmental Catalysis and Health Risk Control, Institute of Environmental Health and Pollution Control, Guangdong University of Technology, Guangzhou 510006, China; Guangzhou Key Laboratory of Environmental Catalysis and Pollution Control, Key Laboratory for City Cluster Environmental Safety and Green Development of the Ministry of Education, School of Environmental Science and Engineering, Guangdong University of Technology, Guangzhou 510006, China*; orcid.org/0000-0002-8641-4276

Guiying Li − *Guangdong-Hong Kong-Macao Joint Laboratory for Contaminants Exposure and Health, Guangdong Key*

https://doi.org/10.1021/jacs.5c04343
J. Am. Chem. Soc. 2025, 147, 34327−34338

Laboratory of Environmental Catalysis and Health Risk Control, Institute of Environmental Health and Pollution Control, Guangdong University of Technology, Guangzhou 510006, China; Guangzhou Key Laboratory of Environmental Catalysis and Pollution Control, Key Laboratory for City Cluster Environmental Safety and Green Development of the Ministry of Education, School of Environmental Science and Engineering, Guangdong University of Technology, Guangzhou 510006, China; orcid.org/0000-0002-6777-4786

Joseph S. Francisco − *Department of Earth and Environmental Science and Department of Chemistry, University of Pennsylvania, Philadelphia, Pennsylvania 19104-6316, United States;* orcid.org/0000-0002-5461-1486

Complete contact information is available at: https://pubs.acs.org/10.1021/jacs.5c04343

Author Contributions

The manuscript was written through contributions of all the authors.

Notes

The authors declare no competing financial interest.

■ ACKNOWLEDGMENTS

This work is supported by the NSFC (42020104001, 42277081 and 42077189), the Basic and Applied Basic Research Fund Project of Guangdong Province (2024A1515012691), National Key Research and Development Program of China (2022YFC3105600), and Guangzhou Science and Technology Program (2025A04J5188).

■ REFERENCES

(1) Zhang, M.; Klimach, T.; Ma, N.; Könemann, T.; Pöhlker, C.; Wang, Z.; Kuhn, U.; Scheck, N.; Pöschl, U.; Su, H.; Cheng, Y. Size-Resolved Single-Particle Fluorescence Spectrometer for Real-Time Analysis of Bioaerosols: Laboratory Evaluation and Atmospheric Measurements. *Environ. Sci. Technol.* **2019**, *53* (22), 13257−13264.

(2) Rohr, A. C.; Wyzga, R. E. Attributing health effects to individual particulate matter constituents. *Atmos. Environ.* **2012**, *62*, 130−152.

(3) Moreno-Ríos, A. L.; Tejeda-Benítez, L. P.; Bustillo-Lecompte, C. F. Sources, characteristics, toxicity, and control of ultrafine particles: An overview. *Geosci. Front.* **2022**, *13* (1), No. 101147.

(4) Zhao, B.; Shrivastava, M.; Donahue, N. M.; Gordon, H.; Schervish, M.; Shilling, J. E.; Zaveri, R. A.; Wang, J.; Andreae, M. O.; Zhao, C.; Gaudet, B.; Liu, Y.; Fan, J.; Fast, J. D. High concentration of ultrafine particles in the Amazon free troposphere produced by organic new particle formation. *Proc. Natl. Acad. Sci. U.S.A.* **2020**, *117* (41), 25344−25351.

(5) Guo, S.; Hu, M.; Peng, J.; Wu, Z.; Zamora, M. L.; Shang, D.; Du, Z.; Zheng, J.; Fang, X.; Tang, R.; Wu, Y.; Zeng, L.; Shuai, S.; Zhang, W.; Wang, Y.; Ji, Y.; Li, Y.; Zhang, A. L.; Wang, W.; Zhang, F.; Zhao, J.; Gong, X.; Wang, C.; Molina, M. J.; Zhang, R. Remarkable nucleation and growth of ultrafine particles from vehicular exhaust. *Proc. Natl. Acad. Sci. U.S.A.* **2020**, *117* (7), 3427−3432.

(6) Yao, L.; Garmash, O.; Bianchi, F.; Zheng, J.; Yan, C.; Kontkanen, J.; Junninen, H.; Mazon, S. B.; Ehn, M.; Paasonen, P.; Sipilä, M.; Wang, M.; Wang, X.; Xiao, S.; Chen, H.; Lu, Y.; Zhang, B.; Wang, D.; Fu, Q.; Geng, F.; Li, L.; Wang, H.; Qiao, L.; Yang, X.; Chen, J.; Kerminen, V.-M.; Petäjä, T.; Worsnop, D. R.; Kulmala, M.; Wang, L. Atmospheric new particle formation from sulfuric acid and amines in a Chinese megacity. *Science* **2018**, *361* (6399), 278−281.

(7) Almeida, J.; Schobesberger, S.; Kürten, A.; Ortega, I. K.; Kupiainen-Määttä, O.; Praplan, A. P.; Adamov, A.; Amorim, A.; Bianchi, F.; Breitenlechner, M.; David, A.; Dommen, J.; Donahue, N. M.; Downard, A.; Dunne, E.; Duplissy, J.; Ehrhart, S.; Flagan, R. C.; Franchin, A.; Guida, R.; Hakala, J.; Hansel, A.; Heinritzi, M.; Henschel, H.; Jokinen, T.; Junninen, H.; Kajos, M.; Kangasluoma, J.; Keskinen, H.; Kupc, A.; Kurtén, T.; Kvashin, A. N.; Laaksonen, A.; Lehtipalo, K.; Leiminger, M.; Leppä, J.; Loukonen, V.; Makhmutov, V.; Mathot, S.; McGrath, M. J.; Nieminen, T.; Olenius, T.; Onnela, A.; Petäjä, T.; Riccobono, F.; Riipinen, I.; Rissanen, M.; Rondo, L.; Ruuskanen, T.; Santos, F. D.; Sarnela, N.; Schallhart, S.; Schnitzhofer, R.; Seinfeld, J. H.; Simon, M.; Sipilä, M.; Stozhkov, Y.; Stratmann, F.; Tomé, A.; Tröstl, J.; Tsagkogeorgas, G.; Vaattovaara, P.; Viisanen, Y.; Virtanen, A.; Vrtala, A.; Wagner, P. E.; Weingartner, E.; Wex, H.; Williamson, C.; Wimmer, D.; Ye, P.; Yli-Juuti, T.; Carslaw, K. S.; Kulmala, M.; Curtius, J.; Baltensperger, U.; Worsnop, D. R.; Vehkamäki, H.; Kirkby, J. Molecular understanding of sulphuric acid−amine particle nucleation in the atmosphere. *Nature* **2013**, *502* (7471), 359−363.

(8) Kirkby, J.; Curtius, J.; Almeida, J.; Dunne, E.; Duplissy, J.; Ehrhart, S.; Franchin, A.; Gagné, S.; Ickes, L.; Kürten, A.; Kupc, A.; Metzger, A.; Riccobono, F.; Rondo, L.; Schobesberger, S.; Tsagkogeorgas, G.; Wimmer, D.; Amorim, A.; Bianchi, F.; Breitenlechner, M.; David, A.; Dommen, J.; Downard, A.; Ehn, M.; Flagan, R. C.; Haider, S.; Hansel, A.; Hauser, D.; Jud, W.; Junninen, H.; Kreissl, F.; Kvashin, A.; Laaksonen, A.; Lehtipalo, K.; Lima, J.; Lovejoy, E. R.; Makhmutov, V.; Mathot, S.; Mikkilä, J.; Minginette, P.; Mogo, S.; Nieminen, T.; Onnela, A.; Pereira, P.; Petäjä, T.; Schnitzhofer, R.; Seinfeld, J. H.; Sipilä, M.; Stozhkov, Y.; Stratmann, F.; Tomé, A.; Vanhanen, J.; Viisanen, Y.; Vrtala, A.; Wagner, P. E.; Walther, H.; Weingartner, E.; Wex, H.; Winkler, P. M.; Carslaw, K. S.; Worsnop, D. R.; Baltensperger, U.; Kulmala, M. Role of sulphuric acid, ammonia and galactic cosmic rays in atmospheric aerosol nucleation. *Nature* **2011**, *476* (7361), 429−433.

(9) Brean, J.; Dall'Osto, M.; Simó, R.; Shi, Z.; Beddows, D. C. S.; Harrison, R. M. Open ocean and coastal new particle formation from sulfuric acid and amines around the Antarctic Peninsula. *Nat. Geosci.* **2021**, *14* (6), 383−388.

(10) Olenius, T.; Halonen, R.; Kurtén, T.; Henschel, H.; Kupiainen-Määttä, O.; Ortega, I. K.; Jen, C. N.; Vehkamäki, H.; Riipinen, I. New particle formation from sulfuric acid and amines: Comparison of monomethylamine, dimethylamine, and trimethylamine. *J. Geophys. Res.: Atmos.* **2017**, *122* (13), 7103−7118.

(11) Ge, Y.; Liu, Y.; Chu, B.; He, H.; Chen, T.; Wang, S.; Wei, W.; Cheng, S. Ozonolysis of Trimethylamine Exchanged with Typical Ammonium Salts in the Particle Phase. *Environ. Sci. Technol.* **2016**, *50* (20), 11076−11084.

(12) Li, K.; Jacob, D. J.; Liao, H.; Qiu, Y.; Shen, L.; Zhai, S.; Bates, K. H.; Sulprizio, M. P.; Song, S.; Lu, X.; Zhang, Q.; Zheng, B.; Zhang, Y.; Zhang, J.; Lee, H. C.; Kuk, S. K. Ozone pollution in the North China Plain spreading into the late-winter haze season. *Proc. Natl. Acad. Sci. U.S.A.* **2021**, *118* (10), No. e2015797118.

(13) Chen, Z.-Y.; Petetin, H.; Turrubiates, R. F. M.; Achebak, H.; García-Pando, C. P.; Ballester, J. Population exposure to multiple air pollutants and its compound episodes in Europe. *Nat. Commun.* **2024**, *15* (1), No. 2024.

(14) National Center for Biotechnology Information. PubChem Compound Summary for CID 198133 2024 https://pubchem.ncbi.nlm.nih.gov/compound/Methyl-ammonium-sulfate.

(15) O'Brien, P. J.; Siraki, A. G.; Shangari, N. Aldehyde Sources, Metabolism, Molecular Toxicity Mechanisms, and Possible Effects on Human Health. *Crit. Rev. Toxicol.* **2005**, *35* (7), 609−662.

(16) Tong, D.; Chen, J.; Qin, D.; Ji, Y.; Li, G.; An, T. Mechanism of atmospheric organic amines reacted with ozone and implications for the formation of secondary organic aerosols. *Sci. Total Environ.* **2020**, *737*, No. 139830.

(17) Lim, S.; McArdell, C. S.; von Gunten, U. Reactions of aliphatic amines with ozone: Kinetics and mechanisms. *Water Res.* **2019**, *157*, 514−528.

(18) Li, X.; Li, Y.; Lawler, M. J.; Hao, J.; Smith, J. N.; Jiang, J. Composition of Ultrafine Particles in Urban Beijing: Measurement Using a Thermal Desorption Chemical Ionization Mass Spectrometer. *Environ. Sci. Technol.* **2021**, *55* (5), 2859−2868.

(19) Ma, Y. J.; Xu, Y.; Yang, T.; Xiao, H. W.; Xiao, H. Y. Measurement report: Characteristics of nitrogen-containing organics in PM2.5 in Ürümqi, northwestern China − differential impacts of combustion of

fresh and aged biomass materials. *Atmos. Chem. Phys.* **2024**, *24* (7), 4331−4346.
(20) Choi, N. R.; Ahn, Y. G.; Lee, J. Y.; Kim, E.; Kim, S.; Park, S. M.; Song, I. H.; Shin, H. J.; Kim, Y. P. Particulate Nitrosamines and Nitramines in Seoul and Their Major Sources: Primary Emission versus Secondary Formation. *Environ. Sci. Technol.* **2021**, *55* (12), 7841−7849.
(21) Choi, N. R.; Ahn, Y. G.; Lee, J. Y.; Kim, E.; Kim, S.; Park, S. M.; Song, I. H.; Kim, Y. P. Winter-time particulate nitrosamines and nitramines in the atmosphere at seoul, South Korea. *Atmos. Environ.* **2020**, *237*, No. 117582.
(22) Gui, L.; Xu, Y.; You, Y.-C.; Ma, Y.-J.; Yang, T.; Liu, T.; Xiao, H.-W.; Xiao, H.; Xiao, H.-Y. Oxidative Degradation of Higher-Molecular-Weight Aromatic Amine Compounds Is a Potential Source of Anilinium in Urban Aerosols. *Environ. Sci. Technol. Lett.* **2024**, *11* (12), 1355−1361.
(23) Choi, N. R.; Kim, Y. P.; Lee, J. Y.; Kim, E.; Kim, S.; Shin, H. J. Impact of ozonation on the formation of particulate nitrosodimethylamine (NDMA) in atmosphere. *Chemosphere* **2024**, *349*, No. 140794.
(24) Zahardis, J.; Geddes, S.; Petrucci, G. A. The ozonolysis of primary aliphatic amines in fine particles. *Atmos. Chem. Phys.* **2008**, *8* (5), 1181−1194.
(25) Lee, W.; Na, S.; Seo, C.; Son, H.; Lee, Y. Chlorination of N,N-dimethylhydrazine compounds: reaction kinetics, mechanisms, and implications for controlling N-nitrosodimethylamine formation during ozonation. *Environ. Sci.: Water Res. Technol.* **2020**, *6* (9), 2567−2579.
(26) McCurry, D. L.; Quay, A. N.; Mitch, W. A. Ozone Promotes Chloropicrin Formation by Oxidizing Amines to Nitro Compounds. *Environ. Sci. Technol.* **2016**, *50* (3), 1209−1217.
(27) Muñoz, F.; von Sonntag, C. The reactions of ozone with tertiary amines including the complexing agents nitrilotriacetic acid (NTA) and ethylenediaminetetraacetic acid (EDTA) in aqueous solution. *J. Chem. Soc., Perkin Trans.* **2000**, *2* (10), 2029−2033.
(28) Weller, C.; Herrmann, H. Kinetics of nitrosamine and amine reactions with NO3 radical and ozone related to aqueous particle and cloud droplet chemistry. *Atmos. Res.* **2015**, *151*, 64−71.
(29) Hesske, H.; Gloe, K. Hydration Behavior of Alkyl Amines and Their Corresponding Protonated Forms. 1. Ammonia and Methylamine. *J. Phys. Chem. A* **2007**, *111* (39), 9848−9853.
(30) Ben-Naim, A.; Marcus, Y. Solvation thermodynamics of nonionic solutes. *J. Chem. Phys.* **1984**, *81* (4), 2016−2027.
(31) Qiu, X.; Duan, L.; Gao, J.; Wang, S.; Chai, F.; Hu, J.; Zhang, J.; Yun, Y. Chemical composition and source apportionment of PM10 and PM2.5 in different functional areas of Lanzhou, China. *J. Environ. Sci.* **2016**, *40*, 75−83.
(32) Masiol, M.; Hopke, P. K.; Felton, H. D.; Frank, B. P.; Rattigan, O. V.; Wurth, M. J.; LaDuke, G. H. Analysis of major air pollutants and submicron particles in New York City and Long Island. *Atmos. Environ.* **2017**, *148*, 203−214.
(33) Zhang, Q.; Jimenez, J. L.; Canagaratna, M. R.; Allan, J. D.; Coe, H.; Ulbrich, I.; Alfarra, M. R.; Takami, A.; Middlebrook, A. M.; Sun, Y. L.; Dzepina, K.; Dunlea, E.; Docherty, K.; DeCarlo, P. F.; Salcedo, D.; Onasch, T.; Jayne, J. T.; Miyoshi, T.; Shimono, A.; Hatakeyama, S.; Takegawa, N.; Kondo, Y.; Schneider, J.; Drewnick, F.; Borrmann, S.; Weimer, S.; Demerjian, K.; Williams, P.; Bower, K.; Bahreini, R.; Cottrell, L.; Griffin, R. J.; Rautiainen, J.; Sun, J. Y.; Zhang, Y. M.; Worsnop, D. R. Ubiquity and dominance of oxygenated species in organic aerosols in anthropogenically-influenced Northern Hemisphere midlatitudes. *Geophys. Res. Lett.* **2007**, *34* (13), No. 13801.
(34) Jiang, P.-Y.; Katsumura, Y.; Nagaishi, R.; Domae, M.; Ishikawa, K.; Ishigure, K.; Yoshida, Y. Pulse radiolysis study of concentrated sulfuric acid solutions. Formation mechanism, yield and reactivity of sulfate radicals. *J. Chem. Soc. Faraday Trans.* **1992**, *88* (12), 1653−1658.
(35) Tang, Y.; Thorn, R. P.; Mauldin, R. L.; Wine, P. H. Kinetics and spectroscopy of the SO4− radical in aqueous solution. *J. Photochem. Photobiol., A: Chem.* **1988**, *44* (3), 243−258.
(36) Weber, R. J.; Guo, H.; Russell, A. G.; Nenes, A. High aerosol acidity despite declining atmospheric sulfate concentrations over the past 15 years. *Nat. Geosci.* **2016**, *9*, 282−285.
(37) Craig, R. L.; Nandy, L.; Axson, J. L.; Dutcher, C. S.; Ault, A. P. Spectroscopic Determination of Aerosol pH from Acid−Base Equilibria in Inorganic, Organic, and Mixed Systems. *J. Phys. Chem. A* **2017**, *121* (30), 5690−5699.
(38) Karydis, V. A.; Tsimpidi, A. P.; Pozzer, A.; Lelieveld, J. How alkaline compounds control atmospheric aerosol particle acidity. *Atmos. Chem. Phys.* **2021**, *21* (19), 14983−15001.
(39) Cope, J. D.; Bates, K. H.; Tran, L. N.; Abellar, K. A.; Nguyen, T. B. Sulfur radical formation from the tropospheric irradiation of aqueous sulfate aerosols. *Proc. Natl. Acad. Sci. U.S.A.* **2022**, *119* (36), No. e2202857119.
(40) VandeVondele, J.; Krack, M.; Mohamed, F.; Parrinello, M.; Chassaing, T.; Hutter, J. Quickstep: Fast and accurate density functional calculations using a mixed Gaussian and plane waves approach. *Comput. Phys. Commun.* **2005**, *167* (2), 103−128.
(41) Kühne, T. D.; Iannuzzi, M.; Ben, M. D.; Rybkin, V. V.; Seewald, P.; Stein, F.; Laino, T.; Khaliullin, R. Z.; Schütt, O.; Schiffmann, F.; Golze, D.; Wilhelm, J.; Chulkov, S.; Bani-Hashemian, M. H.; Weber, V.; Borštnik, U.; Taillefumier, M.; Jakobovits, A. S.; Lazzaro, A.; Pabst, H.; Müller, T.; Schade, R.; Guidon, M.; Andermatt, S.; Holmberg, N.; Schenter, G. K.; Hehn, A.; Bussy, A.; Belleflamme, F.; Tabacchi, G.; Glöß, A.; Lass, M.; Bethune, I.; Mundy, C. J.; Plessl, C.; Watkins, M.; VandeVondele, J.; Krack, M.; Hutter, J. CP2K: An electronic structure and molecular dynamics software package - Quickstep: Efficient and accurate electronic structure calculations. *J. Chem. Phys.* **2020**, *152* (19), No. 194103.
(42) Becke, A. D. Density-functional exchange-energy approximation with correct asymptotic behavior. *Phys. Rev. A* **1988**, *38* (6), No. 3098.
(43) Lee, C.; Yang, W.; Parr, R. G. Development of the Colle-Salvetti correlation-energy formula into a functional of the electron density. *Phys. Rev. B* **1988**, *37* (2), No. 785.
(44) Grimme, S. Accurate description of van der Waals complexes by density functional theory including empirical corrections. *J. Comput. Chem.* **2004**, *25* (12), 1463−1473.
(45) Grimme, S.; Antony, J.; Ehrlich, S.; Krieg, H. A consistent and accurate ab initio parametrization of density functional dispersion correction (DFT-D) for the 94 elements H-Pu. *J. Chem. Phys.* **2010**, *132* (15), No. 154104.
(46) Grimme, S. Semiempirical GGA-type density functional constructed with a long-range dispersion correction. *J. Comput. Chem.* **2006**, *27* (15), 1787−1799.
(47) VandeVondele, J.; Hutter, J. Gaussian basis sets for accurate calculations on molecular systems in gas and condensed phases. *J. Chem. Phys.* **2007**, *127* (11), No. 114105.
(48) Hartwigsen, C.; Goedecker, S.; Hutter, J. Relativistic separable dual-space Gaussian pseudopotentials from H to Rn. *Phys. Rev. B* **1998**, *58* (7), No. 3641.
(49) Goedecker, S.; Teter, M.; Hutter, J. Separable dual-space Gaussian pseudopotentials. *Phys. Rev. B* **1996**, *54* (3), 1703−1710.
(50) Agarwal, B.; Jürschik, S.; Sulzer, P.; Petersson, F.; Jaksch, S.; Jordan, A.; Märk, T. D. Detection of isocyanates and polychlorinated biphenyls using proton transfer reaction mass spectrometry. *Rapid Commun. Mass Spectrom.* **2012**, *26* (8), 983−989.
(51) Stönner, C.; Derstroff, B.; Klüpfel, T.; Crowley, J. N.; Williams, J. Glyoxal measurement with a proton transfer reaction time of flight mass spectrometer (PTR-TOF-MS): characterization and calibration. *J. Mass Spectrom.* **2017**, *52* (1), 30−35.
(52) Yuan, B.; Koss, A. R.; Warneke, C.; Coggon, M.; Sekimoto, K.; de Gouw, J. A. Proton-Transfer-Reaction Mass Spectrometry: Applications in Atmospheric Sciences. *Chem. Rev.* **2017**, *117* (21), 13187−13229.
(53) Kim, J.; Choe, Y. J.; Kim, S. H.; Jeong, K. Enhancing the decomposition of refractory contaminants on SO42–functionalized iron oxide to accommodate surface SO4- generated via radical transfer from OH. *Appl. Catal., B* **2019**, *252*, 62−76.
(54) Møller, K. H.; Berndt, T.; Kjaergaard, H. G. Atmospheric Autoxidation of Amines. *Environ. Sci. Technol.* **2020**, *54* (18), 11087−11099.

https://doi.org/10.1021/jacs.5c04343
J. Am. Chem. Soc. 2025, 147, 34327−34338

(55) Onel, L.; Blitz, M.; Dryden, M.; Thonger, L.; Seakins, P. Branching Ratios in Reactions of OH Radicals with Methylamine, Dimethylamine, and Ethylamine. *Environ. Sci. Technol.* **2014**, *48* (16), 9935−9942.
(56) Alam, M. A.; Ren, Z.; da Silva, G. Nitramine and nitrosamine formation is a minor pathway in the atmospheric oxidation of methylamine: A theoretical kinetic study of the CH_3NH+O_2 reaction. *Int. J. Chem. Kinet.* **2019**, *51* (9), 723−728.
(57) Zhang, X.; Lu, B.; Zhang, J.; Fu, X.; Deng, H.; Qiao, L.; Ding, C.; Gao, F. Experimental and simulation study on hydroxyl group promoting low-temperature oxidation of active groups in coal. *Fuel* **2023**, *340*, No. 127501.
(58) Biswas, S.; Shukla, P. K. Reactions of chlorophyll with hydroxyl radicals via RAF, HAT and SET mechanisms: A theoretical study. *Struct. Chem.* **2024**, *35*, 1905−1916.
(59) Yang, X.; Tao, Y.; Murphy, J. G. Kinetics of the oxidation of ammonia and amines with hydroxyl radicals in the aqueous phase. *Environ. Sci.:Processes Impacts* **2021**, *23* (12), 1906−1913.
(60) Simić, M.; Neta, P.; Hayon, E. Pulse radiolytic investigation of aliphatic amines in aqueous solution. *Int. J. Radiat. Phys. Chem.* **1971**, *3* (3), 309−320.
(61) Li, M.; Karu, E.; Brenninkmeijer, C.; Fischer, H.; Lelieveld, J.; Williams, J. Tropospheric OH and stratospheric OH and Cl concentrations determined from CH4, CH3Cl, and SF6 measurements. *npj Clim. Atmos. Sci.* **2018**, *1* (1), No. 29.
(62) Bunkan, A. J. C.; Tang, Y.; Sellevåg, S. R.; Nielsen, C. J. Atmospheric Gas Phase Chemistry of CH2 = NH and HNC. A First-Principles Approach. *J. Phys. Chem. A* **2014**, *118* (28), 5279−5288.
(63) Shen, Q.; Liu, Y. D.; Zhong, R. Degradation mechanisms of simple aliphatic amines under ozonation: a DFT study. *Environ. Sci.:Processes Impacts* **2021**, *23* (3), 480−490.
(64) Xu, Y.; Dong, X.-N.; Xiao, H.-Y.; Zhou, J.-X.; Wu, D.-S. Proteinaceous Matter and Liquid Water in Fine Aerosols in Nanchang, Eastern China: Seasonal Variations, Sources, and Potential Connections. *J. Geophys. Res.: Atmos.* **2022**, *127* (15), No. e2022JD036589.
(65) Zhang, Q.; Wang, Y.; Liu, M.; Zheng, M.; Yuan, L.; Liu, J.; Tao, S.; Wang, X. Wintertime Formation of Large Sulfate Particles in China and Implications for Human Health. *Environ. Sci. Technol.* **2023**, *57* (48), 20010−20023.
(66) Akbar Ali, M.; M, B.; Lin, K. C. Catalytic effect of a single water molecule on the OH + CH2NH reaction. *Phys. Chem. Chem. Phys.* **2018**, *20* (6), 4297−4307.
(67) Shannon, R. J.; Blitz, M. A.; Goddard, A.; Heard, D. E. Accelerated chemistry in the reaction between the hydroxyl radical and methanol at interstellar temperatures facilitated by tunnelling. *Nat. Chem.* **2013**, *5* (9), 745−749.
(68) George, I. J.; Abbatt, J. P. D. Heterogeneous oxidation of atmospheric aerosol particles by gas-phase radicals. *Nat. Chem.* **2010**, *2* (9), 713−722.
(69) Nielsen, C. J.; Herrmann, H.; Weller, C. Atmospheric chemistry and environmental impact of the use of amines in carbon capture and storage (CCS). *Chem. Soc. Rev.* **2012**, *41* (19), 6684−6704.
(70) Dong, V. M.; Fiedler, D.; Carl, B.; Bergman, R. G.; Raymond, K. N. Molecular Recognition and Stabilization of Iminium Ions in Water. *J. Am. Chem. Soc.* **2006**, *128* (45), 14464−14465.
(71) Dong, Z.; Francisco, J. S.; Long, B. Ammonolysis of Glyoxal at the Air-Water Nanodroplet Interface. *Angew. Chem., Int. Ed.* **2024**, *63* (6), No. e202316060.
(72) Kong, X.; Castarède, D.; Thomson, E. S.; Boucly, A.; Artiglia, L.; Ammann, M.; Gladich, I.; Pettersson, J. B. C. A surface-promoted redox reaction occurs spontaneously on solvating inorganic aerosol surfaces. *Science* **2021**, *374* (6568), 747−752.
(73) Zhang, W.; Zhong, J.; Shi, Q.; Gao, L.; Ji, Y.; Li, G.; An, T.; Francisco, J. S. Mechanism for Rapid Conversion of Amines to Ammonium Salts at the Air−Particle Interface. *J. Am. Chem. Soc.* **2021**, *143* (2), 1171−1178.
(74) Yin, R.; Li, X.; Yan, C.; Cai, R.; Zhou, Y.; Kangasluoma, J.; Sarnela, N.; Lampilahti, J.; Petäjä, T.; Kerminen, V. M.; Bianchi, F.; Kulmala, M.; Jiang, J. Revealing the sources and sinks of negative cluster ions in an urban environment through quantitative analysis. *Atmos. Chem. Phys.* **2023**, *23* (9), 5279−5296.
(75) Singh, S. K.; Zhu, C.; La Jeunesse, J.; Fortenberry, R. C.; Kaiser, R. I. Experimental identification of aminomethanol (NH_2CH_2OH)—the key intermediate in the Strecker Synthesis. *Nat. Commun.* **2022**, *13* (1), No. 375.
(76) Feldmann, M. T.; Widicus, S. L.; Blake, G. A.; Kent, D. R. I. V.; Goddard, W. A., III Aminomethanol water elimination: Theoretical examination. *J. Chem. Phys.* **2005**, *123* (3), No. 034304.
(77) Ashraful, A. M.; da Silva, G. A detailed chemical kinetic model for the supercritical water oxidation of methylamine: The importance of imine formation. *Int. J. Chem. Kinet.* **2020**, *52* (10), 701−711.
(78) Ali, M. A. Computational studies on the gas phase reaction of methylenimine (CH2NH) with water molecules. *Sci. Rep.* **2020**, *10* (1), No. 10995.
(79) Chapleski, R. C.; Zhang, Y.; Troya, D.; Morris, J. R. Heterogeneous chemistry and reaction dynamics of the atmospheric oxidants, O3, NO3, and OH, on organic surfaces. *Chem. Soc. Rev.* **2016**, *45* (13), 3731−3746.
(80) Wadia, Y.; Tobias, D. J.; Stafford, R.; Finlayson-Pitts, B. J. Real-Time Monitoring of the Kinetics and Gas-Phase Products of the Reaction of Ozone with an Unsaturated Phospholipid at the Air−Water Interface. *Langmuir* **2000**, *16* (24), 9321−9330.
(81) Adeney, P. D.; Bouma, W. J.; Radom, L.; Rodwell, W. R. Nitrosomethane and its nitrone and oxime isomers. A theoretical study of 1,2- and 1,3-intramolecular hydrogen shifts. *J. Am. Chem. Soc.* **1980**, *102* (12), 4069−4074.
(82) Liang, G.-M.; Ren, Y. I.; Chu, S.-Y.; Wong, N.-B. Exploring the potential energy surface of the catalyzed isomerization of nitrosomethane to formaldoxime. *J. Theor. Comput. Chem.* **2007**, *06* (01), 187−195.
(83) Wang, T.; Xue, L.; Brimblecombe, P.; Lam, Y. F.; Li, L.; Zhang, L. Ozone pollution in China: A review of concentrations, meteorological influences, chemical precursors, and effects. *Sci. Total Environ.* **2017**, *575*, 1582−1596.
(84) He, C.; Liu, J.; Zhou, Y.; Zhou, J.; Zhang, L.; Wang, Y.; Liu, L.; Peng, S. Synergistic $PM_{2.5}$ and O_3 control to address the emerging global $PM_{2.5}$-O_3 compound pollution challenges. *Eco-Environ. Health* **2024**, *3* (3), 325−337.
(85) Lee, J. K.; Samanta, D.; Nam, H. G.; Zare, R. N. Micrometer-Sized Water Droplets Induce Spontaneous Reduction. *J. Am. Chem. Soc.* **2019**, *141* (27), 10585−10589.
(86) Li, K.; Guo, Y.; Nizkorodov, S. A.; Rudich, Y.; Angelaki, M.; Wang, X.; An, T.; Perrier, S.; George, C. Spontaneous dark formation of OH radicals at the interface of aqueous atmospheric droplets. *Proc. Natl. Acad. Sci. U.S.A.* **2023**, *120* (15), No. e2220228120.
(87) Lee, J. K.; Walker, K. L.; Han, H. S.; Kang, J.; Prinz, F. B.; Waymouth, R. M.; Nam, H. G.; Zare, R. N. Spontaneous generation of hydrogen peroxide from aqueous microdroplets. *Proc. Natl. Acad. Sci. U.S.A.* **2019**, *116* (39), 19294−19298.

https://doi.org/10.1021/jacs.5c04343
J. Am. Chem. Soc. 2025, 147, 34327−34338